Multichannel Monte Carlo Singular Spectrum Analysis With Colored Noise Assessment: Application to Greenland GNSS Vertical Displacement

Fatemeh Esmaeili, Hamid Mehrabi, Seyed Mohsen Khazraei, and Alireza Amiri-Simkooei

***Abstract*—Permanent GNSS stations continuously monitor Earth's crust movements in horizontal and vertical directions. The recorded data include deterministic variations, including linear trends, periodic signals, and offsets, alongside stochastic variations represented by various noise models. Accurately detecting deterministic behaviors depends on a realistic estimation of the observation noise model. A new multivariate algorithm based on Monte Carlo singular spectrum analysis (MCSSA) is developed to analyze the multiple channels of time-series data simultaneously (e.g., different position components or data from multiple stations), considering noise correlations without being limited to a specific noise model. Testing on simulated GNSS data showed that, by increasing the number of channels, the algorithm could accurately identify dominant annual and semiannual components in the presence of colored noise. The results also indicated that unrealistic assumptions about the GNSS position time-series noise model can be misleading in the MCSSA hypothesis testing. Applying the algorithm to real Greenland GNSS data confirmed the significance of annual and semiannual harmonic patterns when white plus flicker noise (FLWN) combinations were considered as the stochastic behavior of data. In the univariate analysis of the vertical position time series contaminated with random walk noise, none of the annual and semiannual signals were interpreted to be significant. At the same time, the proposed multivariate algorithm successfully identified the annual signal but lacked sufficient channels (stations) to confirm the significance of the semiannual signal in the presence of random walk noise. The multivariate analysis has confirmed the significance of semiannual signal across 21 time series contaminated with FLWN, which univariate analysis missed due to a high level of colored noise.**

***Index Terms*—Greenland GNSS stations, multichannel Monte Carlo singular spectrum analysis (MCSSA), multivariate time-series analysis, significant signals identification.**

Received 22 December 2024; revised 8 April 2025 and 25 June 2025; accepted 2 August 2025. Date of publication 5 August 2025; date of current version 27 August 2025. *(Corresponding author: Alireza Amiri-Simkooei.)*

Fatemeh Esmaeili and Hamid Mehrabi are with the Department of Geomatics Engineering, Faculty of Civil Engineering and Transportation, University of Isfahan, Isfahan 8174673441, Iran.

Seyed Mohsen Khazraei is with the Department of Surveying Engineering, Faculty of Civil Engineering, Jundi-Shapur University of Technology, Dezful 6461618674, Iran.

Alireza Amiri-Simkooei is with the Department of Control and Operations, Faculty of Aerospace Engineering, Delft University of Technology, 2629 Delft, The Netherlands, and also with the Department of Geomatics Engineering, Faculty of Civil Engineering and Transportation, University of Isfahan, Isfahan 8174673441, Iran (e-mail: a.amirisimkooei@tudelft.nl).

Digital Object Identifier 10.1109/JSTARS.2025.3596164

I. Introduction

THE Earth's surface is in a constant state of response to various forces. In Greenland, alongside other geophysical phenomena, the main deformations arise from the postglacial rebound and changes in ice mass. The GNSS network stations mounted on the rocky margin of Greenland offer an ideal platform for studying the Earth's response to such phenomena [1]. They provide us with daily GNSS station position time series, which is called GNSS data hereafter.

The secular uplift trend, seasonal (annual and semiannual) variations, and occasional transient signals have been observed in many studies investigating these GNSS data. These variations are usually studied to quantify the elastic and viscoelastic response of the Earth's surface to the mentioned phenomena [2], [3].

Precise modeling of seasonal variations is essential for studying mass cycles and surface components, such as the atmosphere [2], [3], [4]. Mismodeling these variations can introduce uncertainties in estimating Greenland's secular uplift trend, primarily driven by ongoing ice mass loss. These variations are often compared with regional climate models and ice mass loading data [1], [5]. A review of previous studies on GNSS position time series in Greenland reveals a strong interest in using multichannel singular spectrum analysis(M-SSA) to identify geophysical and geological signals [1], [2]. But what drives this interest?

First, seasonal variations in Greenland station positions are likely irregular in phase and amplitude. These time-varying seasonal signals have recently been noticed in the GNSS position time series [6], [7]. In Arctic regions, the ice mass distribution causes the crustal deformation to change over time. The amount of ice melting in a particular area can vary from year to year [8], causing the amount of mass loaded and unloaded in that location to fluctuate [9]. Moreover, other external mass components, including the atmosphere and water, may impose similar irregularities [2].

Second, Greenland's regional geophysical and environmental processes result in common modes in site positions. The significant spatial correlation between different stations for individual components over short baselines is reported by the authors in [10] and [11]. Accordingly, the simultaneous analysis of GNSS data of adjacent stations cannot only be useful to retrieve

common-mode signals [6] but also essential to truly handle the common-mode errors (CMEs) [12]. However, to avoid misleading results, the similarity of signal and noise structures must be investigated in advance.

Chen et al. [13] were the first to apply SSA to the GNSS position time series, extracting time-variable seasonal components of the GNSS position time series. The efficiency of SSA for this purpose was further supported by the authors in [6] and [14]. Various contributions have addressed enhancements in classical SSA methodology. Noteworthy, among these are the improved SSA algorithm proposed by Ji et al. [15] capable of handling time series with missing data, and extended SSA, developed by Ji et al. [16] for processing incomplete heterogeneous geodetic time series, and the adaptive SSA proposed by Li et al. [17], which addresses the problem of setting the embedded window size and selecting the principal components (PCs).

The multichannel singular spectrum analysis (M-SSA) is a multivariate data-adaptive technique that can facilitate the extraction of seasonal signals with variations in phase and amplitudes, while its multichannel analysis feature enhances the detection of common signals originating from common imposing phenomena [18]. M-SSA was also successfully employed by the authors in [19] and [20] to retrieve common transient deformations and seasonal signals from the GNSS position time series. Consequently, it was used as an appropriate technique to study Greenland GNSS data [1], [2]. However, the use of SSA should be approached with caution in the presence of colored noise and it is crucial to explore strategies for discriminating between signals and noise.

Since the late 1990s, many research articles have shown that the stochastic behaviors of GNSS position time series, commonly referred to as noise, can be approximated by a linear combination of white noise (W) and power-law (PL) processes [10], [21], [22]. This combination can be further defined using three specific models: white noise (WN), flicker noise (FL), and random walk (RW), which correspond to spectral indices of 0, 1, and 2, respectively [23], [24]. In recent years, researchers have employed the generalized Gauss–Markov with white noise model (GGMWN) to model the stochastic behavior of GNSS station time series. This approach has significantly reduced uncertainty in estimating the linear trends of these series [23], [24], [25], [26], [27]. He et al. [27] analyzed 110 globally distributed IGS stations, indicating that the stochastic characteristics of the vertical component for 13% of these stations are better described by GGMWN noise model than the standard PL plus WN. However, modeling the stochastic behavior of GNSS stations with GGMWN noise model results in a complex and nonlinear variance estimation issue [26].

The colored noise in the GNSS position time series has already proved to mimic periodic patterns or produce spurious variations in signal phase and amplitudes [14]. It can consequently be absorbed by the main SSA eigenmodes and lead to the misinterpretation of variations in the amplitude and phase of the signal [28]. This issue may be neglected in many research articles that employ data-adaptive methods.

Monte Carlo singular spectrum analysis (MCSSA) was first proposed by Allen and Smith [28] to prevent misrepresentation of the stochastic behaviors as significant signals. They introduced a significance test versus the null hypothesis of the first-order autoregressive noise process AR (1). The method was then extended to the multichannel form by Allen and Robertson [29]. Despite all modifications to MCSSA by Groth and Ghil [30], its main shortcoming was that it was not simply applicable to any arbitrary noise combination existing in the data.

MCSSA was first applied to the GNSS position time series by Xu and Yue [14], without modifying the noise hypothesis (AR(1) noise), to extract significant time-varying seasonal variations. However, they pointed out that this approach may be misleading in the presence of flicker and RW noise. Walwer et al. [19] conduct MCSSA on GNSS position time series with the null hypothesis of WN plus PL. The authors in [1] and [5] used a common approach to study seasonal and transient signals in Greenland. Besides that, they have not provided a straightforward algorithm for generating surrogate data; their algorithm is still restricted to a combination of WN and PL noise with a spectral index.

Khazraei and Amiri-Simkooei [31] proposed a general MCSSA algorithm that is not limited to any kind of stochastic model. In their algorithm, the noise components are estimated using the least-squares variance component estimation (LS-VCE) method, followed by the generation of surrogate data through Cholesky decomposition. They have represented and generated noise models using the well-known linear combination of cofactor matrices and (co)variance components. The algorithm was run on single-channel GNSS data assuming the white noise plus flicker noise (FLWN) model as the dominant noise in most GNSS position time series. However, it is not restricted to FLWN and can be simply implemented in the presence of RW noise (as it is observed in some of the Greenland GNSS stations); there is still a need for additional formulations to incorporate its multichannel mode.

In Greenland, the GNSS position time series are mostly contaminated with white and flicker noise. The RW, however, contributes to some stations. Zhang et al. [5] conducted an MCSSA analysis against the null hypothesis of a PL plus WN model. The spectral index of the PL noise in this study ranged from 0.7 to 0.8. Bian et al. [32] utilized the maximum likelihood estimation method to determine the CME in the vertical component of GNSS stations in Greenland, proposing the FLWN combination as the primary noise model for these stations. The FLWN model was also identified as the most suitable model for Greenland's GNSS stations in [33]. Furthermore, both [32] and [33] studies confirmed a stochastic behavior consistent with the white noise, flicker noise, and random walk noise (RWFLWN) model for a limited number of GNSS stations in the Greenland region.

All mentioned backgrounds and especially the case study of Greenland in which a network of GNSS stations is influenced by common modes with strong spatial correlation motivated us to extend the MCSSA algorithm using LS–VCE and Cholesky decomposition to a multichannel mode. The proposed multichannel MCSSA algorithm can cover all defects of the existing MCSSA algorithms. It can be applied to multichannel analysis, is not restricted to any specific noise combination, and can consider between-series correlation while generating surrogate data.

The objectives of this article are outlined as follows:

1) to formulate a comprehensive multichannel MCSSA algorithm capable of application to time series without any restrictions;
2) to highlight the importance of using realistic noise structure in MCSSA tests;
3) to represent the importance of multichannel analysis in extracting common-mode signals and noise while exploring whether the simultaneous analysis of more channels results in an enhanced interpretation of these modes;
4) the GNSS vertical component time series from 24 stations located in Greenland are analyzed using the proposed algorithm.

The stations are categorized based on their underlying noise structure FLWN or RWFLWN and the algorithm effectiveness is examined for both groups.

The rest of this article is organized as follows. First, the essential methodology of M-SSA required to develop the MC-SSA into the multivariate mode is provided in Section II. In Section III, the MCSSA algorithm proposed by Khazraei and Amiri-Simkooei [31], using LS-VCE and Cholesky decomposition, is developed in multichannel mode. In Section IV, a preanalysis is then conducted to gain insights into the study area and the available data. Section V involves validating the proposed algorithm by using completely supervised simulated data. Then, in Section VI, the Greenland GNSS data are analyzed using the multichannel MCSSA, and the numerical results are provided and discussed. In Section VII, the pros and cons of the algorithm are summarized. The results of the article are discussed in Section VIII. Finally, Section IX concludes this article.

II. Multichannel SSA

M-SSA is a tool for simultaneous analysis of time series with similar dynamic structures. The fundamental methodologies of M-SSA are provided in this section. For more details, refer to Ghil et al.'s article [18]. M-SSA involves two main steps: decomposition and reconstruction.

A. Decomposition

Let $\boldsymbol{Y} = [y_i(t) : i = 1, \ldots, r; t = 1, \ldots, m]$ be an $m \times r$ multivariate set of time series with r channels of m length. Setting M as the SSA window length, the starting point of M-SSA is to form the following $rM \times rM$ block matrix $\tilde{\boldsymbol{T}}_{\boldsymbol{Y}}$

$$\tilde{\boldsymbol{T}}_{\boldsymbol{Y}} = \begin{bmatrix} \boldsymbol{T}_{1,1} & \boldsymbol{T}_{1,2} & \cdots & \boldsymbol{T}_{1,r} \\ \boldsymbol{T}_{2,1} & \boldsymbol{T}_{2,2} & \cdots & \boldsymbol{T}_{2,r} \\ \vdots & \vdots & \ddots & \vdots \\ \boldsymbol{T}_{r,1} & \boldsymbol{T}_{r,2} & \cdots & \boldsymbol{T}_{r,r} \end{bmatrix}. \tag{1}$$

The block $\boldsymbol{T}_{i,i'}$ represents the $M \times M$ lag covariance matrix between channels i and i', where $i,i' = 1, \ldots, r$. The entry $(T_{i,i'})_{j,j'}$ of this matrix is the cross covariance between channels i and i' at lag $\tau = j - j'$, where $j, j' = 1, \ldots M$ (the lag ranges from 0 to $M - 1$). These cross covariances can be estimated using the following estimator:

$$(T_{i,i'})_{j,j'} = \frac{1}{\tilde{N}} \sum_{t\,=\,\max(1,1+j-j')}^{\min(m,m+j-j')} y_i(t)\, y_{i'}(t+j-j') \tag{2}$$

where $\tilde{N} = \min(m, m+j-j') - \max(1, 1+j-j')$. The lag covariance matrix $\tilde{\boldsymbol{T}}_{\boldsymbol{Y}}$ is then diagonalized using the eigenvalue decomposition

$$\boldsymbol{\Lambda} = \boldsymbol{E}^T \tilde{\boldsymbol{T}}_{\boldsymbol{Y}} \boldsymbol{E} \tag{3}$$

where $\boldsymbol{\Lambda}$ is a diagonal matrix of the eigenvalues λ_k and $\boldsymbol{E}$ contains the eigenvectors $\boldsymbol{E}^k$ on its columns; $k = 1, \ldots, rM$. Each eigenvector $\boldsymbol{E}^k$ is composed of r segments with the length of M corresponding to each channel. These single-channel $M \times 1$ eigenvectors, known as the empirical orthogonal functions, are denoted by $\boldsymbol{E}_i^k$, $i = 1, \ldots, r$.

B. Reconstruction

In M-SSA, the kth PC $\boldsymbol{A}^k$ is computed as follows:

$$A^k(t) = \sum_{j=1}^{M} \sum_{i=1}^{r} y_i(t+j-1)\, E_i^k(j) \tag{4}$$

and the kth reconstructed component (RC) for the ith channel $\boldsymbol{R}_i^k$ is then obtained through the following equation:

$$R_i^k(t) = \frac{1}{M_t} \sum_{j\,=L_t}^{U_t} A^k(t-j+1)\, E_i^k(j). \tag{5}$$

The lower and upper bounds of summation, L_t and U_t, and the normalization factor M_t are given by Plaut and Vautard [34]

$$L_t, U_t, M_t) = \begin{cases} (1, t, t) & \text{for } 1 \le t \le M-1 \\ (1, M, M) & \text{for } M \le t \le m-M+1 \\ (t-m+M, M, m-t+1) & \text{for } m-M+2 \le t \le m. \end{cases} \tag{6}$$

Indexing a group of eigenmodes by a set of indices $\mathcal{K} \subseteq \{1, \ldots, rM\}$, $\boldsymbol{R}_i^{\mathcal{K}} = \sum_{k \epsilon \mathcal{K}} \boldsymbol{R}_i^k$ reconstructs the group total variation in channel i, e.g., a pair of sequential eigenmodes with indices $\mathcal{K} = \{k_1, k_2\}$ with a common eigenvector dominant frequency can reconstruct a periodic pattern.

III. Multichannel MCSSA

In this section, we introduce a multichannel MCSSA algorithm, a generalized version of the algorithm proposed by Khazraei and Amiri-Simkooei [31]. The algorithm employs multivariate LS-VCE for noise modeling, and it also estimates and incorporates the correlation between channels when formulating the null hypothesis. This is one of the main concerns in multichannel MCSSA to avoid misinterpreting eigenmodes [30]. The surrogate data are generated using Cholesky decomposition, following the single-channel formulation. This approach ensures that the statistical behavior of the surrogate data closely resembles that of the noise present in the original data. This is mathematically proven by elaborating on the multivariate

covariance matrix, Cholesky decomposition, and error propagation law. The proposed algorithm consists of the following three steps.

A. Estimating the Covariance Matrix Using Multivariate LS-VCE

Recall the multichannel time series $\boldsymbol{Y}$, introduced prior to (1), the following equation can be put forward as the multivariate linear model for observation equations

$$E\ (\mathrm{vec}\,(\boldsymbol{Y})) = (\boldsymbol{I_r} \otimes \boldsymbol{A})\ \mathrm{vec}\,(\boldsymbol{X}) \tag{7}$$

where E, vec, and $\otimes$ are the expectation operator, the vector operator, and the Kronecker product, respectively. $\boldsymbol{I_r}$ represents an identity matrix of size r, $\boldsymbol{A}$ represents the $m \times n$ design matrix of a single time series, and $\boldsymbol{X}$ represents the $n \times r$ matrix of unknowns, where n is the number of unknowns in the functional model of a single time series. Neglecting the periodicities in the time series, the unknowns can be restricted to time-series intercepts and linear rates with the design matrix $\boldsymbol{A}$ of size $m \times 2$ [35].

The covariance matrix of the multichannel time series $\boldsymbol{Y}$, denoted by $\boldsymbol{Q}_{\mathrm{vec}(\boldsymbol{Y})}$, which is an $mr \times mr$ matrix, can also be formulated as follows:

$$\boldsymbol{Q}_{\mathrm{vec}(\boldsymbol{Y})} = D\,(\mathrm{vec}\,(\boldsymbol{Y})) = \boldsymbol{\Sigma} \otimes \boldsymbol{Q} = \boldsymbol{\Sigma} \otimes \sum_{l=1}^{p} \sigma_l \boldsymbol{Q}_l \tag{8}$$

where D is the dispersion operator. $\boldsymbol{Q}$ is an $m \times m$ matrix that represents the temporal correlation in the time series and is modeled as a linear combination of the known cofactor matrices $\boldsymbol{Q}_l$, $l = 1, \ldots, p$ corresponding to the underlying noise models in the GNSS data, e.g., white, flicker, and RW noise. σ_l, $l = 1, \ldots, p$ are the unknown (co)variance components under estimation. $\boldsymbol{\Sigma}$ is an $r \times r$ matrix that characterizes the between-series (spatial) correlation of the time series and needs to be estimated.

If the assumed stochastic model for the data is limited to WN, FLWN, or combined RWFLWN, then (8) will be transformed into the respective forms (9), (10), and (11)

$$\boldsymbol{Q}_{\mathrm{vec}(\boldsymbol{Y})} = D\ (\mathrm{vec}\,(\boldsymbol{Y})) = \boldsymbol{\Sigma} \otimes \left(\sigma^2_{\mathrm{WN}} \mathbf{I}\right) \tag{9}$$

$$\boldsymbol{Q}_{\mathrm{vec}(\boldsymbol{Y})} = D\ (\mathrm{vec}\,(\boldsymbol{Y})) = \boldsymbol{\Sigma} \otimes \left(\sigma^2_{\mathrm{WN}} \mathbf{I} + \sigma^2_{\mathrm{FL}} \boldsymbol{Q}_{\mathrm{FL}}\right) \tag{10}$$

$$\boldsymbol{Q}_{\mathrm{vec}(\boldsymbol{Y})} = D\,(\mathrm{vec}\,(\boldsymbol{Y})) = \boldsymbol{\Sigma} \otimes \left(\sigma^2_{\mathrm{WN}} \mathbf{I} + \sigma^2_{\mathrm{FL}} \boldsymbol{Q}_{\mathrm{FL}} + \sigma^2_{\mathrm{RW}} \boldsymbol{Q}_{\mathrm{RW}}\right). \tag{11}$$

In these equations, σ_{WN} , σ_{FL} , and σ_{RW} denote the unknown (co)variance components of the white noise, flicker noise, and random walk noise, respectively. The cofactor matrix of the WN is the identity matrix ($\mathbf{I}$), while the $\boldsymbol{Q}_{\mathrm{FL}}$ and $\boldsymbol{Q}_{\mathrm{RW}}$—the cofactor matrices of the FL and RW noise—are calculated using the following equations [36]:

$$\boldsymbol{Q}_{\mathrm{PL}} = \Delta T^{\frac{\alpha}{2}}\ U^T U \tag{12}$$

$$\boldsymbol{U} = \begin{bmatrix} h_0 & h_1 & \cdots & h_N \\ 0 & h_0 & \cdots & h_{N-1} \\ \vdots & \vdots & \ddots & \vdots \\ 0 & 0 & \cdots & h_0 \end{bmatrix} \tag{13}$$

$$h_i = \left(\frac{\alpha}{2} + i - 1\right) \frac{h_{i-1}}{i},\ \ h_0 = 1. \tag{14}$$

The subscript PL denotes the PL noise and α is the PL spectral index. $\alpha = 1$ represents the flicker noise and $\alpha = 2$ corresponds to the RW noise. ΔT is the sampling rate of the time series.

The unknown (co)variance components σ_l and the unknown matrix of between-series correlations can be estimated using the multivariate LS-VCE algorithm [35]. Arranging the unknown variance components σ_l in a vector as $\boldsymbol{\sigma} = [\sigma_1 \quad \sigma_2 \quad \ldots \quad \sigma_p]^T$, its least-squares estimator reads

$$\hat{\boldsymbol{\sigma}} = \boldsymbol{N}^{-1}\, \boldsymbol{l} \tag{15}$$

where $\boldsymbol{N}$ and $\boldsymbol{l}$ entries are calculated from (16) and (17) for $i, j = 1, 2, \ldots, p$

$$n_{ij} = \frac{r}{2}\ \mathrm{tr}\left(\boldsymbol{Q}^{-1} \boldsymbol{P}^{\perp}_{\boldsymbol{A}} \boldsymbol{Q}_i \boldsymbol{Q}^{-1} \boldsymbol{P}^{\perp}_{\boldsymbol{A}} \boldsymbol{Q}_j\right) \tag{16}$$

$$l_i = \frac{m-n}{2}\ \mathrm{tr}\left(\hat{\boldsymbol{E}}^T \boldsymbol{Q}^{-1} \boldsymbol{Q}_i \boldsymbol{Q}^{-1} \hat{\boldsymbol{E}} \left(\hat{\boldsymbol{E}}^T \boldsymbol{Q}^{-1} \hat{\boldsymbol{E}}\right)^{-1}\right). \tag{17}$$

In these equations, tr is the trace operator, $\hat{\boldsymbol{E}} = \boldsymbol{P}^{\perp}_{\boldsymbol{A}}\, \boldsymbol{Y}$ is the least-squares residual matrix, and $\boldsymbol{P}^{\perp}_{\boldsymbol{A}} = \boldsymbol{I} - \boldsymbol{A}(\boldsymbol{A}^T \boldsymbol{Q}^{-1} \boldsymbol{A})^{-1} \boldsymbol{A}^T \boldsymbol{Q}^{-1}$ is an orthogonal projector. The covariance matrix $\boldsymbol{Q}$ on the right side of the above equations implies an iterative procedure for estimating the variance components. The between-series covariance matrix $\boldsymbol{\Sigma}$ can finally be estimated as follows:

$$\widehat{\sum} = \frac{\hat{\boldsymbol{E}}^T \boldsymbol{Q}^{-1} \hat{\boldsymbol{E}}}{m-n}. \tag{18}$$

The thorough iterative algorithm of multivariate LS-VCE is presented in [35, Fig. 1].

The noise assessment and, accordingly, estimating the covariance matrix can be more efficiently conducted using the nonnegative LS-VCE (NNLS-VCE) [37]. NNLS-VCE automatically estimates the amplitude of a noise model to be zero when it is unlikely to be present. The algorithm, thus, directly specifies the structure of the noise among the ones presented in (9)–(11). For the detailed algorithm of NNLS-VCE, the readers need to refer to [37].

B. Generating Surrogate Data Through Cholesky Decomposition

Having estimated the positive-definite matrices $\boldsymbol{\Sigma}$ and $\boldsymbol{Q}$, they can be decomposed as follows:

$$\boldsymbol{\Sigma} = \boldsymbol{L_\Sigma}\, \boldsymbol{L_\Sigma^T} \text{ and } \boldsymbol{Q} = \boldsymbol{L_Q}\, \boldsymbol{L_Q^T} \tag{19}$$

where $\boldsymbol{L_\Sigma}$ and $\boldsymbol{L_Q}$ are the lower triangular matrices in the Cholesky decomposition [38]. D series of surrogate data $\boldsymbol{Y}_{Rd}$, $d = 1, \ldots, D$, with r channels of length m, can then be

generated as follows:

$$\boldsymbol{Y}_{Rd} = \boldsymbol{L_Q}\, \boldsymbol{Z}_d \boldsymbol{L}_{\boldsymbol{\Sigma}}^T \tag{20}$$

where $\boldsymbol{Z}_d = [\boldsymbol{z}_{d,1} \quad \boldsymbol{z}_{d,2} \quad \dots \quad \boldsymbol{z}_{d,r}], d = 1, \dots, D$ are the arrays of r standard normally distributed random vectors $\boldsymbol{z}_{d,i}$, $i = 1, \dots, r$ with length m ($\boldsymbol{z}_{d,i} \sim N(0,1)$).

The surrogate data $\boldsymbol{Y}_{Rd}$ can be proved to have the same covariance matrix as the original dataset

$$\boldsymbol{Q}_{\mathrm{vec}(\boldsymbol{Y}_{Rd})} = \boldsymbol{Q}_{\mathrm{vec}(\boldsymbol{Y})} = \boldsymbol{\Sigma} \otimes \boldsymbol{Q} \tag{21}$$

For the sake of brevity, in this section, the reader is referred to [39, Appendix A] to find the properties that hold for the vec operator and Kronecker product [see (A.1)–(A.14)]. Let us start by applying the vec operator to (20). Using (A.13), the equation can be reformulated as follows:

$$\mathrm{vec}\,(\boldsymbol{Y}_{Rd}) = \mathrm{vec}\left(\boldsymbol{L_Q} \boldsymbol{Z}_d \boldsymbol{L}_{\boldsymbol{\Sigma}}^T\right) = (\boldsymbol{L}_{\boldsymbol{\Sigma}} \otimes \boldsymbol{L_Q})\ \mathrm{vec}\,(\boldsymbol{Z}_d)\,. \tag{22}$$

By applying the error propagation law [40] and using the Kronecker product properties (A.9), the covariance matrix of the surrogate data $\boldsymbol{Q}_{\mathrm{vec}(\boldsymbol{Y}_{Rd})}$reads

$$\boldsymbol{Q}_{\mathrm{vec}(\boldsymbol{Y}_{Rd})} = (\boldsymbol{L}_{\boldsymbol{\Sigma}} \otimes \boldsymbol{L_Q})\ \boldsymbol{Q}_{\mathrm{vec}(\boldsymbol{Z}_d)} \left(\boldsymbol{L}_{\boldsymbol{\Sigma}}^T \otimes \boldsymbol{L}_{\boldsymbol{Q}}^T\right). \tag{23}$$

The covariance matrix of the standard normally distributed random vectors $\boldsymbol{z}_{d,i}$ is known to be the $m \times m$ identity matrix $\boldsymbol{I}_m$. Since the generated random vectors are uncorrelated in pairs, it follows that $\boldsymbol{Q}_{\mathrm{vec}(\boldsymbol{Z}_d)} = \boldsymbol{I}_r \otimes \boldsymbol{I}_m$. Equation (23) can, thus, be rewritten as follows:

$$\boldsymbol{Q}_{\mathrm{vec}(\boldsymbol{Y}_{Rd})} = (\boldsymbol{L}_{\boldsymbol{\Sigma}} \otimes \boldsymbol{L_Q})\,(\boldsymbol{I}_r \otimes \boldsymbol{I}_m)\left(\boldsymbol{L}_{\boldsymbol{\Sigma}}^T \otimes \boldsymbol{L}_{\boldsymbol{Q}}^T\right). \tag{24}$$

This can be simplified to

$$\boldsymbol{Q}_{\mathrm{vec}(\boldsymbol{Y}_{Rd})} = \boldsymbol{L}_{\boldsymbol{\Sigma}}\, \boldsymbol{L}_{\boldsymbol{\Sigma}}^T \otimes \boldsymbol{L_Q} \boldsymbol{L}_{\boldsymbol{Q}}^T \tag{25}$$

using another property of the Kronecker product (A.5). Substituting (19) into (25) is the final step to prove (21). The described routine, thus, generates an ensemble of surrogate data with the same stochastic behavior as the original data. The lag covariance matrix $\tilde{\boldsymbol{T}}_{\boldsymbol{Rd}}$ can then be determined for each realization using (1) and (2).

C. Forming the Confidence Intervals

Having calculated the lag covariance matrix $\tilde{\boldsymbol{T}}_{Rd}$ of each series of the surrogate data, they are projected on the eigenvectors of the original data $\boldsymbol{E}$

$$\boldsymbol{\Lambda}_{Rd}^{(\boldsymbol{E})} = \boldsymbol{E}^T\, \tilde{\boldsymbol{T}}_{Rd} \boldsymbol{E} \tag{26}$$

The $\boldsymbol{\Lambda}_{Rd}^{(\boldsymbol{E})}$is not necessarily diagonal, but its diagonal entries $\{\lambda_k^{Rd} : k = 1, \dots, rM\}$ yield the resemblance between the partial variance in the null hypothesis and the original data in the eigendirection of $\boldsymbol{E}$. The confidence intervals are constructed using the diagonal entries of $\boldsymbol{\Lambda}_{Rd}^{(\boldsymbol{E})}$. These intervals are derived from the empirical distribution of the simulated data. Forming empirical confidence intervals based on percentiles is a nonparametric approach to estimate confidence bounds directly from a series of sample data. This method is particularly useful when the underlying distribution is unknown or does not conform to parametric assumptions. According to the theoretical basis of this approach, an eigenvalue from the data is considered statistically significant at the $(1-\alpha)\%$ level if it falls outside the central $(1-\alpha)\%$ portion of the surrogate eigenvalues. This signifies that the observed data eigenvalue differs substantially from those generated by the stochastic noise model in the surrogate realizations under the null hypothesis. In this study, a confidence level of 95% was consistently used across all sections to evaluate the significance of the results. Specifically, the acceptance region of the null hypothesis for any eigenvalue is the interval between the 2.5th and 97.5th percentiles of its corresponding surrogate eigenvalues.

IV. Study Area and GNSS Data Preanalysis

Greenland is the world's largest noncontinental island, located between latitudes 59° and 83°N, and longitudes 11° and 74°W. The Greenland ice sheet covers 81% of the island. Given its unique geophysical characteristics and environmental challenges, Greenland serves as a critical case study for researchers studying ice mass changes and the response of solid Earth to them [41]. Greenland crustal displacement is currently being monitored with 60 GNSS stations installed mostly on bedrock along the coast of Greenland. For this study, GNSS position time series were obtained from the Nevada Geodetic Laboratory (NGL) at the University of Nevada, Reno [42]. The time series are the final 24-hour solutions of IGS14, presented in tenv3 format. The solutions were derived from basic observations at a 5-min rate using GipsyX Version 1.0 software, with a cutoff angle of 7°. Wet and dry tropospheric corrections were interpolated from the VMF1 grid model. The first-order ionospheric corrections were removed using a combination of LC and PC observations, while the second-order corrections were removed by modeling using IONEX data with IGRF12. Tidal corrections were applied based on IERS 2010 conventions, while nontidal corrections were not applied to the observations. The GNSS position time-series dataset has been shown to exhibit significant WN and flicker noise correlations at large scales. Gobron et al. [43] analyzed the NGL dataset and demonstrated that, approximately, 70% of the flicker noise is associated with large-scale variations, likely due to orbit modeling errors. They also observed an increase in the spatial correlations of WN at distances less than 50 km, with this effect being most pronounced in the vertical component.

We chose 24 stations that have integrated time-series data spanning from 2015 to 2022 in order not to deal with the missing data. We may provide the reader with some recommended references that address gap filling in the presence of missing data [44], [45]. The time series of the vertical coordinate component of these stations are analyzed because they are mostly affected in response to ice mass loading activities [1]. Fig. 1 depicts the distribution of the selected stations.

A valid estimation of stochastic noise components in a time series requires the detection and adaptation of offsets that may arise from tectonic movements, changes in GNSS equipment, or human errors during GNSS data processing [25]. In the preprocessing step, the algorithm proposed by

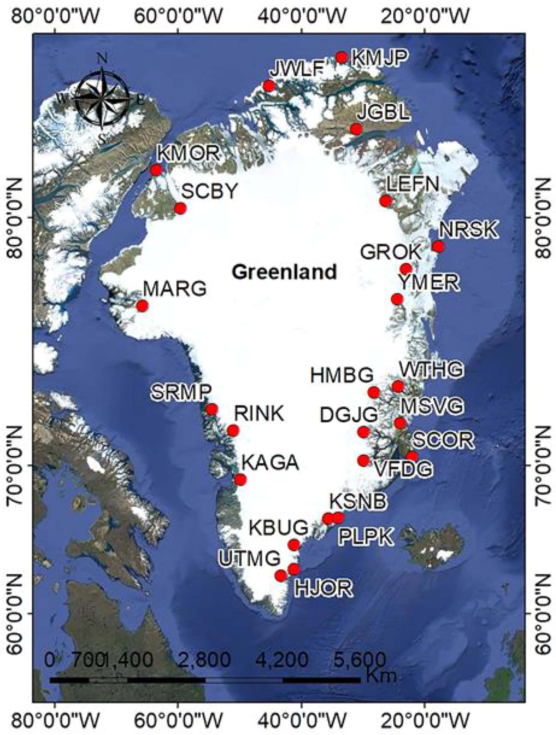

Fig. 1. Distribution of the 24 selected GNSS stations in Greenland.

Amiri-Simkooei et al. [46] is employed to identify and eliminate offsets in the time series. This algorithm is grounded in a mathematical framework that considers two hypotheses: the presence and absence of an offset. The performance of these hypotheses is assessed using the generalized likelihood ratio statistical test. Rejecting the null hypothesis of no offset supports the alternative hypothesis that an offset exists. The significant offsets in the time series are, thus, detected and adapted.

We then conducted a preanalysis to gather insights regarding the range of the amplitudes of annual and semiannual signals and the contribution of the conventional noise models (W, FL, and RW) and their amplitudes for the vertical component time series of each station. The preanalysis was conducted in univariate mode to identify each station's deterministic and stochastic characteristics separately.

The NNLS-VCE method was used to characterize the stochastic model of the time series. The NNLS-VCE automatically estimates the amplitude of a noise model to be zero when it is unlikely to be present [37]. The least-squares estimate of the signal amplitudes was also determined when the covariance matrix of the observations was calculated. Fig. 2 displays annual and semiannual signal amplitudes for these stations. Fig. 3 presents the estimated noise amplitudes. In 3 stations out of 24, nonzero RW variance components were estimated, introducing RWFLWN as the underlying noise combination, while the remaining 21 stations exhibited the FLWN combination. In addition to the presence of RW noise in KBUG, RINK, and KAGA GNSS stations, it was observed that signal amplitudes were relatively small compared with flicker noise amplitudes.

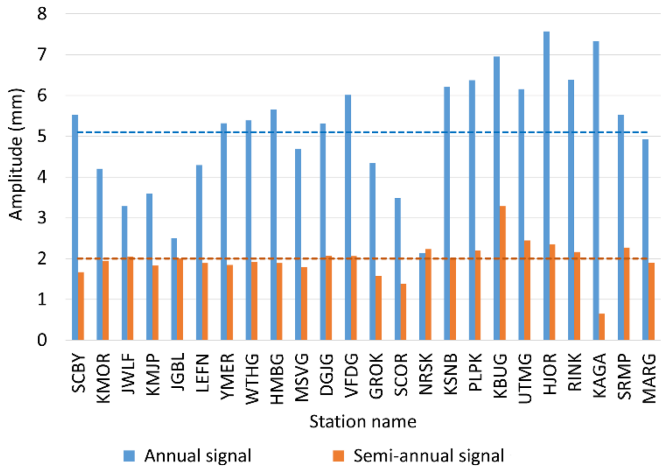

Fig. 2. Amplitudes of annual and semiannual variations in the vertical position time series of Greenland GNSS stations.

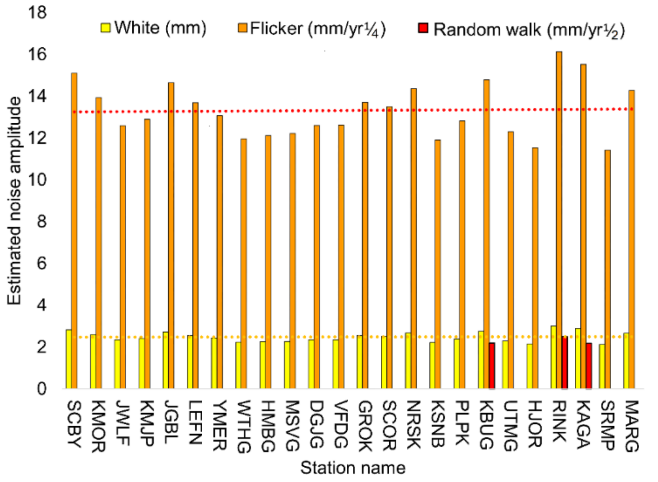

Fig. 3. Estimated amplitudes of noise models for Greenland GNSS stations using univariate NNLS-VCE. The dotted lines are the mean amplitudes of white and flicker noise components.

V. Multichannel MCSSA Validation Using the Simulated Time Series

Before analyzing Greenland GNSS data with the proposed multichannel MCSSA, we organized an instruction to explain how colored noise mimics periodic behaviors in data and to assess the algorithm's effectiveness under various supervised conditions using simulated data. Three sets of simulated data, each consisting of ten channels with varying noise characteristics (FLWN and RWFLWN), were generated for these assessments. All time series are free of intercepts and linear trends. Datasets 1# and 2# incorporate both annual and semiannual signals, while dataset 3# contains only RWFLWN noise without any deterministic behavior. This setup facilitates the specification of eigenvalues and confidence intervals associated with signals. The length of the simulated data, as well as the amplitude of the signals and noise, was determined based on the properties of the preanalyzed Greenland GNSS data (see Figs. 2 and 3), as detailed in Table I. The amplitudes are intentionally fixed to specific values to constrain the effective parameters.

TABLE I
PARAMETERS OF THREE SETS OF SIMULATED TIME SERIES, DATASETS #1–#3, CONTAMINATED WITH FLWN AND RWFLWN

Dataset	Noise combination	Number of channels	Length (years)
#1	FLWN	10	7
#2	RWFLWN	10	7
#3	RWFLWN	10	7

Dataset	Signal amplitude (mm)		Noise amplitude (mm)		
	Annual	Semiannual	W	FL	RW
#1	5	2	2.5	13.5	-
#2	5	2	2.5	13.5	2
#3	-	-	2.5	13.5	2

Dataset #3 is free of deterministic signal.

Two samples of the real Greenland GNSS position time series (SCBY and KAGA stations as samples for FLWN and RWFLWN, respectively) and two samples of the simulated time series of dataset #1 and dataset #2 are depicted in the panels of Fig. 4. An extra semiperiodic pattern (in addition to annual and semiannual) can be observed in the right panels, which are attributed to RW noise.

First, we investigate how the presence of colored noise (flicker and RW) leads to the detection of unrealistic periodic behaviors in data analysis. Next, we examine whether processing multiple channels simultaneously results in more accurate LS-VCE estimates. We then assess whether increasing the number of channels enhances the performance of multichannel MCSSA in capturing significant seasonal variations. Finally, we evaluate the importance of using a realistic noise model in the analysis.

A. Colored Noise Mimic Periodic Behaviors

This section discusses how colored noise in data can mimic periodic behaviors, potentially leading to incorrect interpretations of periodicity in M-SSA analyses. To illustrate this, we analyzed dataset #3 (see Table I) using M-SSA. Dataset #3 contains only stochastic behavior (RWFLWN) and is free of any deterministic behavior. Fig. 5 presents the first 15 eigenvalues from this analysis, along with their corresponding dominant frequencies. As shown in Fig. 5, some components extracted by M-SSA exhibit behaviors similar to seasonal signals with biannual (7th and 9th eigenvalues) and annual (11th and 12th eigenvalues) frequencies, despite the fact that the original simulated data contain no actual periodic behavior.

In order to further investigate the role of the colored noise in imitating periodic behaviors, the noise amplitudes are estimated using NNLS-VCE from the following two data. First, the originally simulated data of dataset #3. Second, the residual data of subtracting the first 15 M-SSA RCs from dataset #3. The estimated amplitudes for ten simulated channels are averaged and presented in Table II. Comparing the results to the simulated amplitudes, as provided in Table I, it can be observed that, removing these 15 RCs reduced the estimated amplitudes of the stochastic noise components, with the amplitude of the RW noise being estimated as zero. This suggests that the semiperiodic components that are identified in the M-SSA analysis of dataset #3 (see Fig. 5) are a part of the colored noise in the data. Accordingly, in the presence of deterministic periodic patterns, colored noise may cause a spurious rise in the eigenvalues of the corresponding modes.

TABLE II
AVERAGE ESTIMATED NOISE AMPLITUDES, USING NNLS-VCE, FOR DATASET #3, BEFORE AND AFTER REMOVAL OF THE FIRST 15 COMPONENTS OBTAINED VIA M-SSA

Dataset #3	Estimated noise amplitude		
	WN (mm)	FL ($\mathrm{mm/yr}^{\frac{1}{4}}$)	RW ($\mathrm{mm/yr}^{\frac{1}{2}}$)
Simulated data	2.38	13.84	0.97
Residual of subtracting 15 components	2.47	13.39	0

B. Multichannel LS-VCE: Impact of Channel Count

To investigate the impact of channel count in VCE, datasets #1 and #2 (each with ten channels) are generated n times. For each simulation, the noise amplitudes in the first channel of each dataset are first estimated using the univariate LS-VCE. The root-mean-square error (RMSE) of these estimations is calculated for all noise components. This routine is then repeated by sequentially adding the next channels and conducting the multivariate LS-VCE until all ten channels are simultaneously analyzed. The estimated RMSEs are plotted in Fig. 6 as bars, against the number of channels included in the multivariate LS-VCE. The accuracy of PL noise estimation using LS-VCE is linked to the noise spectral index. The larger RMSEs for RW noise suggest less accurate estimations due to their nonstationary characteristics. However, the results show that increasing the number of channels improves the estimation of noise variance components, regardless of the noise type. The improvement is particularly pronounced for RW noise; in a multivariate analysis of ten channels, RW noise is estimated nearly five times more accurately than in a univariate analysis.

C. Multichannel MCSSA: Impact of Channel Count

An iterative analysis is once again conducted on datasets #1 and #2 (refer to Table I) to investigate if the use of more channels facilitates the extraction of significant signals. At each iteration, one additional channel is added to the multichannel MCSSA. The optimal value of M strikes a balance between the statistical significance of the extracted modes and the maximum period of the oscillations to be captured [19]. We applied M-SSA with a window length of 700 days throughout the article. This window size has also been selected in previous research to examine

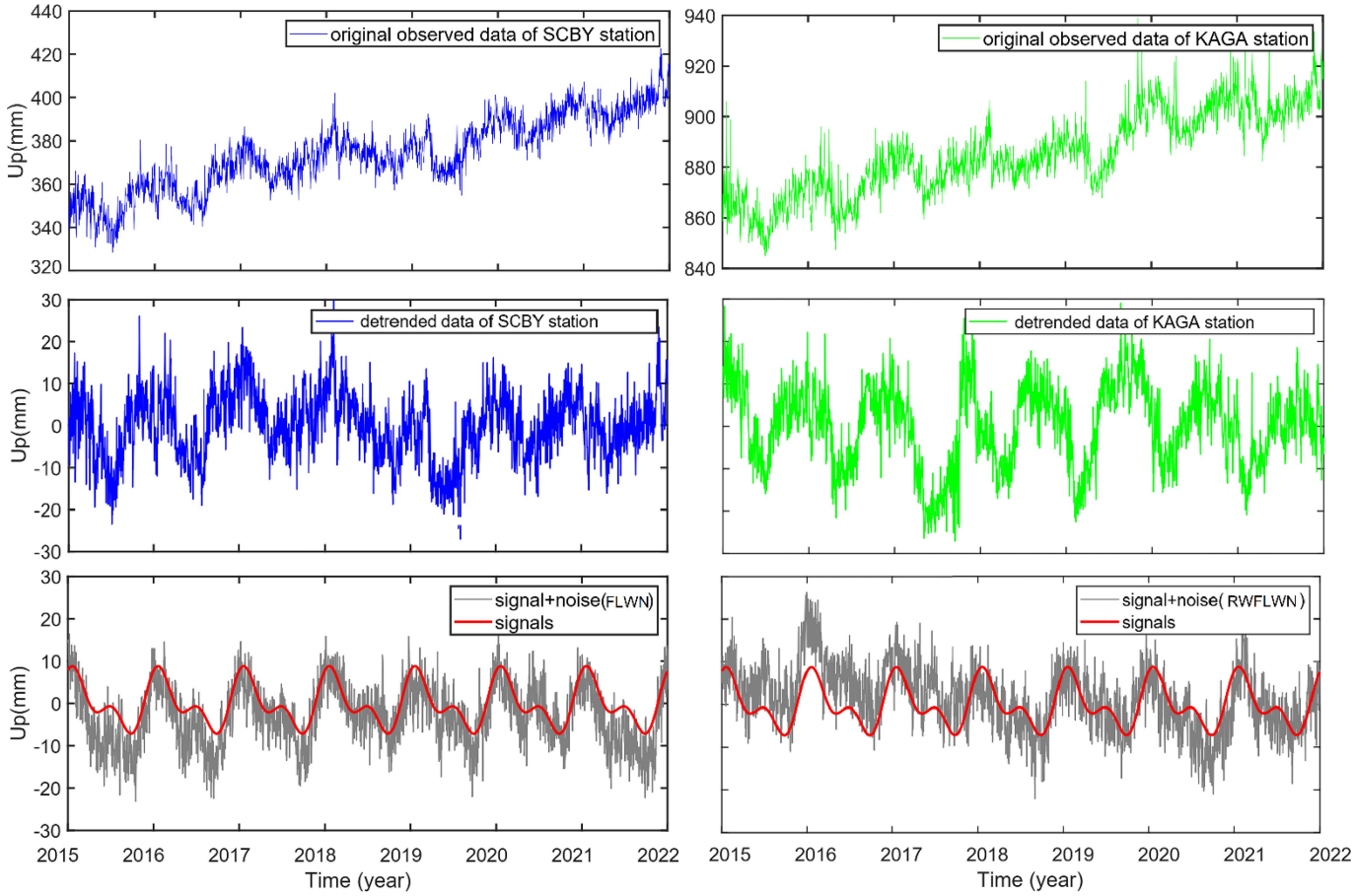

Fig. 4. Original observed data (top panels) and detrended time series (middle panels) of SCBY and KAGA Greenland GNSS station as samples for FLWN and RWFLWN, respectively, and two samples of simulated time series from dataset #1and dataset #2 (bottom panels).

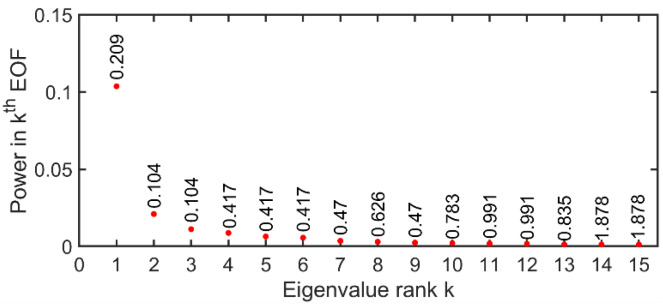

Fig. 5. First 15 eigenvalues from the M-SSA analysis of the simulated dataset #3 (see Table I). The labels are the frequencies associated with the eigenmodes (cycles per year).

seasonal oscillations in the Greenland GNSS position time series by the authors in [1] and [5]. The eigenvalues corresponding to the annual and semiannual signals, along with their 95% confidence intervals, are then obtained. They are depicted in Fig. 7. The two top panels [see Fig. 7(a) and (b)] correspond to dataset #1 contaminated by FLWN, while the two bottom panels [see Fig. 7(c) and (d)] correspond to dataset #2 contaminated by RWFLWN. The eigenvalues corresponding to the annual signals [see Fig. 6(a) and (c)] can be observed to be higher than those of the semiannual signals [see Fig. 7(b) and (d)]. This observation is expected due to the simulated signal amplitudes: 5 mm for annual signals versus 2 mm for semiannual signals.

Inspecting the panels (a) and (b) of Fig. 7, it is observed that a single-channel time series with seven years of data can be sufficient to confirm the significance of the annual and semiannual signals in the simulated data of dataset #1 (with simulating parameters provided in Table I). With the same examination of the results of dataset #2 in panels (c) and (d) of Fig. 7, the indiscernibility of periodic patterns from noise is clearer in the presence of RW noise. However, as the number of channels increases, it can be observed that data eigenvalues tend to go beyond the confidence intervals. The annual and semiannual signals are, respectively, accepted in the MCSSA test when analyzing more than nine and ten channels. Examining the 95% confidence intervals generated from the eigenvalues of the surrogate data, it is also evident that large eigenvalues can be generated by RW noise within this frequency range. Besides the structure of the underlying noise, other factors, including signal-to-noise ratio, the length of the data, spatial correlation, SSA window length, and other underlying signals (in addition to annual and semiannual), can also affect signal reconstruction. These factors can be investigated in later contributions.

As observed in Fig. 7, an increase in the number of channels in the multivariate MCSSA powers up the data eigenvalues. This

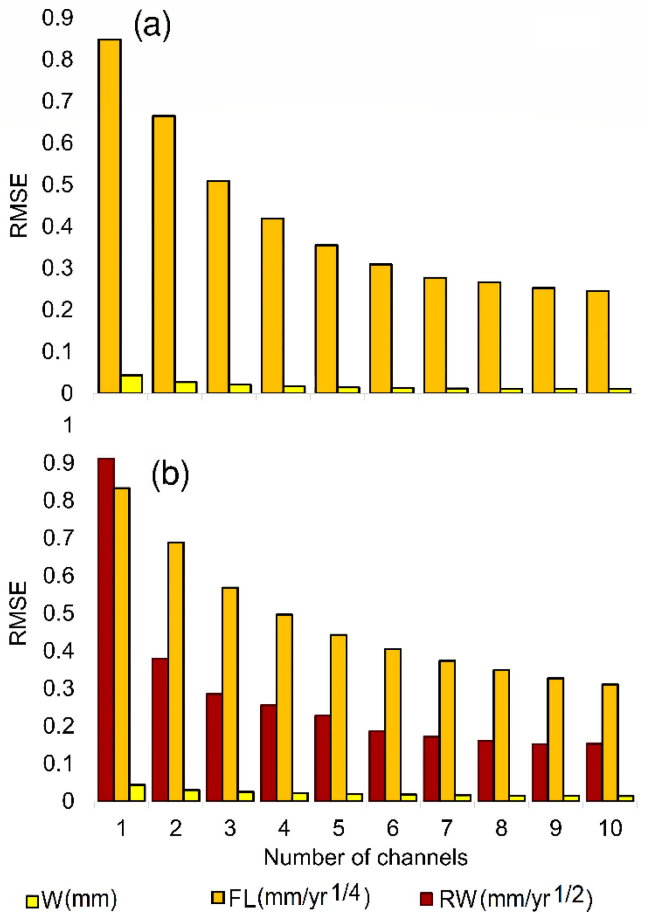

Fig. 6. RMSEs of the estimated noise amplitudes in (a) dataset #1 and (b) dataset #2 (see Table I) against the number of channels included in the multivariate LS-VCE.

amplification can have both positive and negative sides. On the positive side, it validates the effectiveness of M-SSA compared with its single-channel counterpart in extracting common signals. However, on the negative side, it can potentially result in the misinterpretation of random fluctuations. Thus, it highlights the necessity of performing an MCSSA test to guarantee precise and reliable outcomes.

D. Multichannel MCSSA: Unrealistic Assumption of the Noise Model

Khazraei and Amiri-Simkooei [31] discussed the importance of incorporating a realistic noise model into the null hypothesis of the MCSSA significance test to avoid misinterpreting stochastic oscillations as significant periodic patterns. They emphasized that in the presence of PL noise (e.g., a combination of white and flicker noise), conducting the MCSSA test against AR1 noise would be misleading. In this section, we further discuss the issue in multichannel MCSSA, investigating the importance of forming the null hypothesis based on a realistic combination of PL noise. To accomplish this, we focus on dataset #2, which is contaminated by a combination of white, flicker, and RW noise. We test the multichannel SSA-derived eigenmodes

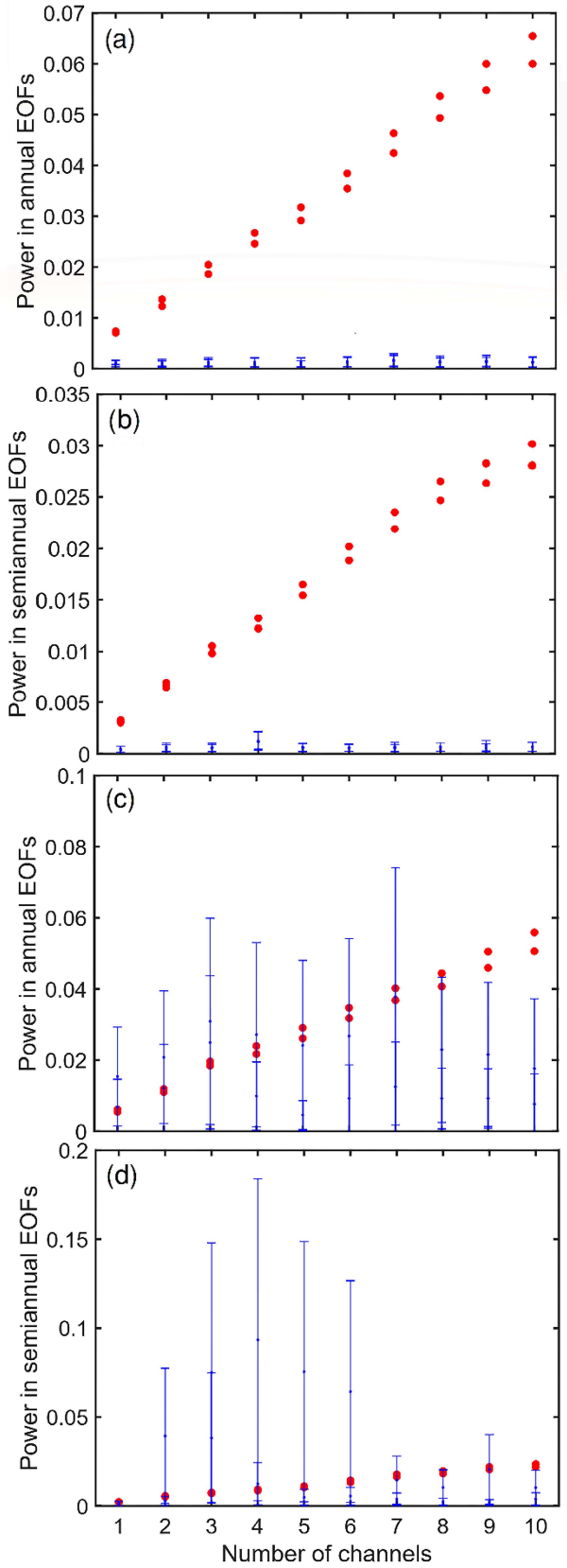

Fig. 7. Eigenvalues and their corresponding 95% confidence intervals of modes associated with annual and semiannual signals for (a) and (b) Datasets #1 and (c) and (d) #2; refer to Table I. At each iteration, one additional channel is added to the multichannel MCSSA.

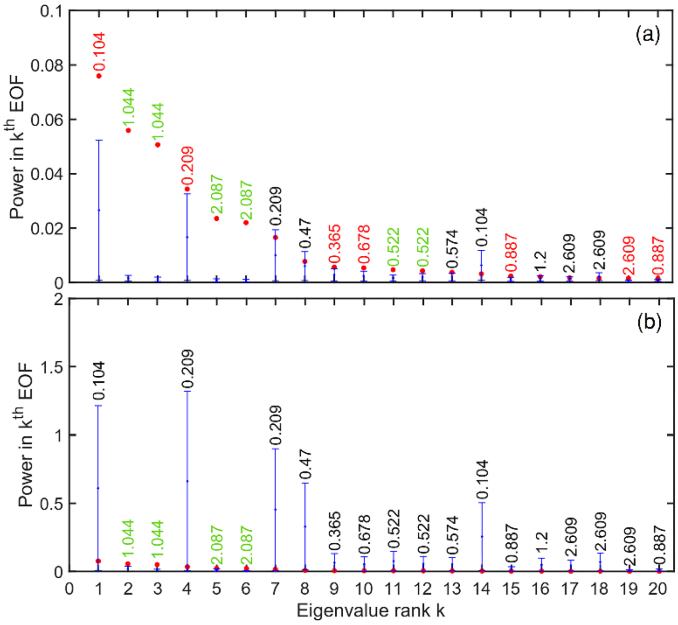

Fig. 8. 95% confidence intervals obtained for simulated dataset #2 (see Table I) against (a) FLWN null hypothesis and (b) RWFLWN null hypothesis. The labels on the confidence intervals are the frequencies associated with the eigenmodes. Red labels indicate frequencies mistakenly interpreted as significant, while green labels indicate frequencies correctly interpreted as significant.

corresponding to this dataset against two different null hypotheses: an unrealistic noise combination of FLWN and a realistic noise combination of RWFLWN.

The results of the tests are provided in Fig. 8. The figure is truncated to the first 20 eigenmodes for better presentation. The labels over the confidence intervals are the frequencies associated with the eigenmodes, computed using the fast Fourier transform of the corresponding eigenvectors, and the green and red labels, respectively, represent the correct or incorrect identification of the eigenmode to be significant. The MCSSA test against the unrealistic noise combination of FLWN guides 7 out of the first 20 eigenvalues mistakenly out of their 95% confidence intervals [see Fig. 8(a)]. This observation implies the presence of stochastic behavior (RW noise) in the original data, which is not considered during the generation of surrogate data.

Considering the correct noise model, two eigenmodes associated with the annual signals (second and third) and two eigenmodes associated with the semiannual signals (fifth and sixth) are correctly interpreted as significant [see Fig. 8(b)]. In this case, none of the first 20 eigenmodes are interpreted mistakenly as significant. The presence of dominant low frequencies with long-term variation in the first 20 eigenmodes (e.g., 0.209 and 0.104 cycles per year), despite the absence of a linear trend, is due to the long-term variations in the RW noise (see Table I). Some of these frequencies are mistakenly interpreted as significant subject to the FLWN null hypothesis [see Fig. 8(a)], while by assuming a realistic RWFLWN model, they are correctly interpreted as not significant [see Fig. 8(b)]. In conclusion, the accurate stochastic model identification of the data and the generation of realistic surrogate data can effectively address the issue of false signal detection in prior studies that have utilized the multichannel MCSSA technique [30].

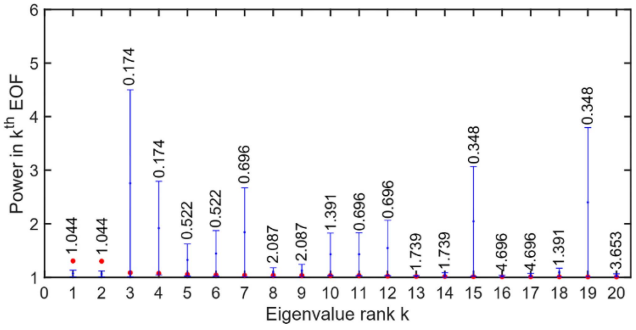

Fig. 9. 95% confidence intervals of the first 20 M-SSA-derived eigenmodes obtained from KBUG, RINK, and KAGA Greenland GNSS position time series against the null hypothesis of RWFLWN. The labels on the confidence intervals are the frequencies associated with the eigenmodes.

VI. Greenland GNSS Data Analysis Using Multichannel MCSSA

The main assumption of any multivariate analysis method is the similarity of the studied time series in common signals and noise models. Based on the preanalysis of GNSS position time-series results, it was found that three stations (KBUG, RINK, and KAGA) are contaminated with the combination of RWFLWN, which differs from the combination of FLWN present in other stations. Given the importance of selecting a realistic noise model for the performance of Monte Carlo tests, as discussed in Section V, the multivariate MCSSA analysis was conducted on the time series of KBUG, RINK, and KAGA stations simultaneously under the null hypothesis of a combined RWFLWN model. Subsequently, 21 other stations were analyzed simultaneously under the null hypothesis of a combined FLWN model.

Fig. 9 shows the M-SSA-derived eigenvalues of three stations, KBUG, RINK, and KAGA, along with their corresponding 95% confidence intervals. The MCSSA test was conducted assuming an RWFLWN combination, and the figure is truncated to the first 20 eigenmodes. Under the assumption of RWFLWN, it is observed that two eigenmodes corresponding to the annual signal (first and second eigenvalues) fall outside their confidence intervals, indicating significance. On the other hand, the two components corresponding to the semiannual signal (eighth and ninth eigenvalues) are within their confidence intervals and are considered not significant. This discrepancy may be due to RW noise, the smaller amplitude of the semiannual signal compared with the annual one (see Fig. 2), and the limited number of analyzed time-series channels. While semiannual harmonic behaviors are commonly observed in GNSS position time series, in the presence of RW noise, more time-series channels with similar characteristics may be necessary to accurately interpret the significance of these signals. The presence of two eigenvalues with a dominant frequency of 0.522 is attributed to the biannual signal.

Three eigenvalues with low dominant frequencies (0.174 and 0.696) are visible among the first ten eigenvalues in Fig. 9.

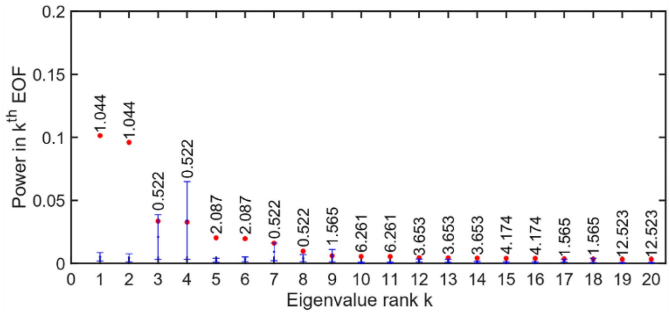

Fig. 10. 95% confidence intervals of the first 20 M-SSA-derived eigenmodes obtained from 21 Greenland GNSS position time series against the null hypothesis of FLWN. The labels on the confidence intervals are the frequencies associated with the eigenmodes.

These frequencies are not present in the MCSSA analysis of 21 other stations (see Fig. 10), indicating that they cannot be attributed to the common harmonic behaviors of GNSS position time series in the region. The presence of these low frequencies may suggest the presence of RW noise in the time series of three stations: KBUG, RINK, and KAGA. It is important to note that colored noise, particularly RW noise, can create patterns that mimic periodic behavior in the data, potentially leading to misinterpretation of harmonic behaviors. The eigenvalues corresponding to these frequencies are not significant under the realistic assumption of RWFLWN.

Fig. 10 depicts the derived eigenvalues from M-SSA analysis for 21 GNSS stations, along with their 95% confidence intervals. It is evident that eigenvalues associated with dominant annual (first and second) and semiannual (fifth and sixth) frequencies fall outside their respective confidence intervals. The presence of an eigenvalue at the dominant frequency of 0.5218 may be attributed to the biannual signal. In addition, in the eigenvalues of the 21 stations with FLWN combination, low frequencies related to RW noise are not observed (see Fig. 10). The significance of eigenvalues corresponding to high-frequency components (10th, 11th and 15th, 16th) could be linked to the harmonics of draconitic signal, which has a frequency of around 1.04 cycle per year [47], [48].

Parallel to the results obtained from the simulated data, it seems necessary to emphasize the importance of considering the contribution of all PL noise models with various spectral indices in MC-SSA. This highlights the feature of the developed MCSSA algorithm, which is not restricted to any combination of noise models.

To further discuss the advantages of the multichannel MC-SSA over its single-channel mode, all stations are analyzed once again using the single-channel MCSSA. The MCSSA tests are conducted against the realistic noise model of each station, RWFLWN for the KBUG, RINK, and KAGA stations, and FLWN for the others. Table III presents the results of the significance test for annual and semiannual eigenpairs. It can be observed that single-channel SSA cannot retrieve pure significant annual and semiannual signals in the presence of RW noise. Both signals are rejected in the significance test for the KBUG, RINK, and KAGA stations. In other stations with

TABLE III
SIGNIFICANCE OF ANNUAL AND SEMIANNUAL SIGNALS USING SINGLE-CHANNEL MCSSA FOR EACH VERTICAL COMPONENT TIME SERIES OF GREENLAND GNSS STATION

#	Station	Signal significance	
		Annual	Semiannual
1	SCBY	✓	×
2	KMOR	✓	×
3	JWLF	✓	✓
4	KMJP	✓	×
5	JGBL	×	×
6	LEFN	✓	×
7	YMER	✓	×
8	WTHG	✓	×
9	HMBG	✓	×
10	MSVG	✓	×
11	DGJG	✓	×
12	VFDG	✓	×
13	GROK	✓	×
14	SCOR	×	×
15	NRSK	×	×
16	KSNB	✓	✓
17	PLPK	✓	×
18	KBUG*	×	×
19	UTMG	✓	×
20	HJOR	✓	×
21	RINK*	×	×
22	KAGA*	×	×
23	SRMP	✓	✓
24	MARG	✓	×

Tests are conducted against RWFLWN combination for stations accompanied by an asterisk (*) and against FLWN combination for other stations.

underlying FLWN, it can also be observed that the semiannual signal is not significant in most stations. Integrating Table III with the noise amplitudes in Fig. 3, it can be inferred that the higher the flicker noise amplitude, the greater the probability of rejecting the annual and semiannual signal.

VII. PROS AND CONS OF THE METHOD

Having verified the algorithm's efficiency using simulated and real GNSS position time series, the main advantages and drawbacks of the algorithm are outlined in the following text.

The effectiveness of time-series analysis methods depends on the data characteristics and the analysis goals.

1) Multichannel MCSSA is indeed a generalized form of SSA. The primary advantage of SSA as a data-adaptive method is its ability to extract time-varying signals.
2) The limited window length in SSA usually results in low spectral resolution, posing challenges in effectively distinguishing adjacent signals.
3) Multichannel SSA is more appropriate for extracting common-mode signals. In addition, common-mode noise can be estimated more accurately using multivariate LS-VCE.
4) On the other side, the station-specific (noncommon) signals may be lost in multichannel analysis. The same scenario holds for noise modeling using multivariate LS-VCE.
5) The latter two considerations play a crucial role in designing a suitable schema for time-series analysis using MCSSA, whether single-channel MCSSA or multichannel MCSSA.
6) Multichannel SSA requires continuous data with the same time intervals across all channels. This can be challenging as different gaps often exist in the time series of various channels. This characteristic often necessitates using gap-filling methods or limits the analysis to short time spans with no missing data in all channels.
7) Compared with the existing MCSSA algorithm, the current algorithm is not restricted to any specific noise structure and can be easily implemented in GNSS position time-series analysis applications.

VIII. Discussion

Previous studies on Greenland GNSS position time series show a strong tendency to use M-SSA as a signal processing method to identify important geophysical and geological patterns, such as seasonal, transient, or long-term changes [1], [2], [5], [7], [9]. The data adaptivity of SSA facilitates the extraction of interannual signals with variations in phase and amplitude. The multichannel analysis feature of M-SSA enhances the detection of common signals originating from common phenomena. Despite the interesting features of M-SSA, it is crucial to explore strategies for discriminating between signals and noise. This contribution aims to address this issue. The multichannel MCSSA algorithm in this article can be used for multichannel analysis and is not limited to any specific type of noise. This article focuses on presenting a simple algorithm clearly for use in GNSS data analysis. Additional investigations were conducted to show the algorithm's performance, which was ultimately used to capture interannual harmonic behaviors of the Greenland GNSS position time series. The analysis of simulated and real GNSS position time series from Greenland stations using multichannel MCSSA yielded impressive results. Three main findings are listed and discussed as follows.

1) Using multivariate LS-VCE to estimate variance components likely provides better results than univariate estimation. An increase in the number of channels in the multivariate analysis also improved accuracy, but this may only hold in a situation where all channels are contaminated with a common noise combination. In addition, the results showed that the accuracy of estimating PL noise with LS-VCE is related to the noise's spectral index.
2) In M-SSA, adding more channels enhances the power of the data eigenvalues. This has both advantages and disadvantages. On the positive side, it demonstrates M-SSAs effectiveness in extracting common signals compared with single-channel methods. On the downside, it may lead to misinterpreting random fluctuations. Therefore, conducting an MCSSA test is essential to ensure the accurate and reliable results.
3) Studies of both simulated data and Greenland GNSS data confirmed that unrealistic noise in the surrogate data of the MCSSA null hypothesis can produce unreliable results. We stressed the importance of including all PL noise models with different spectral indices. Ignoring RW noise in the null hypothesis could make the MCSSA test too lenient, leading to the misidentification of random fluctuations as significant signals. It is important to note that the developed MCSSA algorithm is flexible and not limited to any specific combination of noise models.

IX. Conclusion

The detection of significant variations in GNSS position time series is essential for understanding the unique dynamics of Greenland. This study developed a multichannel MCSSA algorithm that effectively extracts common signals while confirming their statistical significance in the presence of underlying stochastic variations. The stochastic model identification and parameter estimation are conducted using the multivariate LS-VCE, which considers the temporal and spatial correlations in the time series. The consideration of spatial correlation is particularly important in Greenland due to the short baselines involved.

The MCSSA algorithm was applied to simulated time series containing annual and semiannual signals, contaminated by FLWN and RWFLWN models. The results indicate that increasing the number of channels (from one to ten channels) enhances the accuracy of noise component estimation in the multivariate LS-VCE method regardless of the noise type. The enhancement is especially notable for RW noise. In a multivariate analysis involving ten channels, the RW noise is estimated with nearly five times the accuracy of a univariate analysis. Assessing the impact of channel counts on the multichannel MCSSA performance, it was found that a single-channel time series with seven years of data is sufficient to confirm the significance of the annual signal in the simulated dataset contaminated by FLWN. When examining a dataset contaminated by RWFLWN, it becomes clearer that periodic patterns are difficult to distinguish from noise, particularly in the presence of RW noise. However, as the number of channels increases, the data eigenvalues begin to exceed the 95% confidence intervals. The MCSSA test identifies the annual and semiannual signals as significant when analyzing more than nine and ten channels, respectively. To investigate the effect of unrealistic assumptions of the noise model, the

MCSSA test was run versus FLWN null hypothesis for simulated data contaminated by the RWFLWN model. The unrealistic assumption of the noise model reduces the reliability of MCSSA in identifying significant signals.

Applying the developed multichannel MCSSA algorithm to GNSS data from 24 Greenland stations, we found that 3 KBUG, RINK, and KAGA stations were contaminated with RWFLWN combination. The SSA spectrum of these three stations revealed low-frequency eigenmodes not present in the spectrum of the remaining 21 channels contaminated with FLWN. In contrast, the simultaneous analysis of the 21 channels successfully retrieved significant signals, including annual and semiannual signals in the presence of FLWN.

Comparing univariate and multivariate MCSSA results highlighted the effectiveness of the latter, as none of the annual and semiannual common signals were deemed significant under univariate analysis in the presence of the RWFLWN combination. This underscores the advantages of multivariate analysis in detecting common signals in GNSS position time-series data.

References

[1] W. Li et al., "Contributions of Greenland GPS observed deformation from multisource mass loading induced seasonal and transient signals," *Geophysical Res. Lett.*, vol. 47, no. 15, 2020, Art. no. e2020GL088627, doi: 10.1029/2020GL088627.

[2] L. Liu, S. A. Khan, T. van Dam, J. H. Y. Ma, and M. Bevis, "Annual variations in GPS-measured vertical displacements near Upernavik Isstrøm (Greenland) and contributions from surface mass loading," *J. Geophysical Res., Solid Earth*, vol. 122, no. 1, pp. 677–691, 2017, doi: 10.1002/2016JB013494.

[3] K. Nielsen et al., "Crustal uplift due to ice mass variability on Upernavik Isstrøm, west Greenland," *Earth Planet. Sci. Lett.*, vol. 353, pp. 182–189, 2012, doi: 10.1016/j.epsl.2012.08.024.

[4] Y. Li, K. Yang, S. Gao, L. C. Smith, X. Fettweis, and M. Li, "Surface meltwater runoff routing through a coupled supraglacial-proglacial drainage system, Inglefield Land, northwest Greenland," *Int. J. Appl. Earth Observ. Geoinf.*, vol. 106, 2022, Art. no. 102647, doi: 10.1016/j.jag.2021.102647.

[5] B. Zhang, L. Liu, S. A. Khan, T. van Dam, E. Zhang, and Y. Yao, "Transient variations in glacial mass near Upernavik Isstrøm (west Greenland) detected by the combined use of GPS and GRACE data," *J. Geophysical Res., Solid Earth*, vol. 122, no. 12, pp. 10626–10642, 2017, doi: 10.1002/2017JB014529.

[6] A. Klos, M. S. Bos, and J. Bogusz, "Detecting time-varying seasonal signal in GPS position time series with different noise levels," *GPS Solutions*, vol. 22, 2018, Art. no. 21, doi: 10.1007/s10291-017-0686-6.

[7] W. Agnieszka and K. Dawid, "Modeling seasonal oscillations in GNSS time series with complementary ensemble empirical mode decomposition," *GPS Solutions*, vol. 26, no. 4, 2022, Art. no. 101, doi: 10.1007/s10291-022-01288-2.

[8] I. M. Howat, Y. Ahn, I. Joughin, M. R. van den Broeke, J. T. M. Lenaerts, and B. Smith, "Mass balance of Greenland's three largest outlet glaciers, 2000–2010," *Geophysical Res. Lett.*, vol. 38, no. 12, 2011, Art. no. L12501, doi: 10.1029/2011GL047565.

[9] B. Zhang et al., "Geodetic measurements reveal short-term changes of glacial mass near Jakobshavn Isbræ (Greenland) from 2007 to 2017," *Earth Planet Sci. Lett.*, vol. 503, pp. 216–226, 2018, doi: 10.1016/j.epsl.2018.09.029.

[10] S. D. P. Williams et al., "Error analysis of continuous GPS position time series," *J. Geophysical Res., Solid Earth*, vol. 109, no. B3, 2004, Art. no. B03412, doi: 10.1029/2003JB002741.

[11] A. Amiri-Simkooei and C. Tiberius, "Assessing receiver noise using GPS short baseline time series," *GPS Solutions*, vol. 11, pp. 21–35, 2007.

[12] A. R. Amiri-Simkooei, T. H. Mohammadloo, and D. Argus, "Multivariate analysis of GPS position time series of JPL second reprocessing campaign," *J. Geodesy*, vol. 91, pp. 685–704, 2017, doi: 10.1007/s00190-016-0991-9.

[13] Q. Chen, T. van Dam, N. Sneeuw, X. Collilieux, M. Weigelt, and P. Rebischung, "Singular spectrum analysis for modeling seasonal signals from GPS time series," *J. Geodyn.*, vol. 72, pp. 25–35, Dec. 2013, doi: 10.1016/j.jog.2013.05.005.

[14] C. Xu and D. Yue, "Monte Carlo SSA to detect time-variable seasonal oscillations from GPS-derived site position time series," *Tectonophysics*, vol. 665, pp. 118–126, 2015, doi: 10.1016/j.tecto.2015.09.029.

[15] K. Ji, Y. Shen, F. Wang, and Q. Chen, "An efficient improved singular spectrum analysis for processing GNSS position time series with missing data," *Geophysical J. Int.*, vol. 240, no. 1, pp. 189–200, 2025, doi: 10.1093/gji/ggae381.

[16] K. Ji, Y. Shen, Q. Chen, and F. Wang, "Extended singular spectrum analysis for processing incomplete heterogeneous geodetic time series," *J. Geodesy*, vol. 97, no. 8, Aug. 2023, Art. no. 74, doi: 10.1007/s00190-023-01764-8.

[17] C. Li, P. Yang, T. Zhang, and J. Guo, "Periodic signal extraction of GNSS height time series based on adaptive singular spectrum analysis," *Geodesy Geodyn.*, vol. 15, no. 1, pp. 50–60, Jan. 2024, doi: 10.1016/j.geog.2023.04.003.

[18] M. Ghil et al., "Advanced spectral methods for climatic time series," *Rev. Geophys.*, vol. 40, no. 1, pp. 3-1–3-41, 2002, doi: 10.1029/2000RG000092.

[19] D. Walwer, E. Calais, and M. Ghil, "Data-adaptive detection of transient deformation in geodetic networks," *J. Geophysical Res., Solid Earth*, vol. 121, no. 3, pp. 2129–2152, 2016, doi: 10.1002/2015JB012424.

[20] M. Gruszczynska, A. Klos, M. Gruszczyński, and J. Bogusz, "Investigation of time-changeable seasonal components in GPS height time series: A case study for Central Europe," *Acta Geodynamica et Geomaterialia*, vol. 13, pp. 281–289, Apr. 2016, doi: 10.13168/AGG.2016.0010.

[21] A. Santamaría-Gómez and A. Mémin, "Geodetic secular velocity errors due to interannual surface loading deformation," *Geophysical J. Int.*, vol. 202, no. 2, pp. 763–767, 2015.

[22] J. Langbein, "Noise in GPS displacement measurements from Southern California and Southern Nevada," *J. Geophysical Res., Solid Earth*, vol. 113, no. B5, 2008, Art. no. B05405, doi: 10.1029/2007JB005247.

[23] S. Nistor, N.-S. Suba, K. Maciuk, J. Kudrys, E. I. Nastase, and A. Muntean, "Analysis of noise and velocity in GNSS EPN-repro 2 time series," *Remote Sens.*, vol. 13, no. 14, 2021, Art. no. 2783, doi: 10.3390/rs13142783.

[24] R. Hohensinn, P. Ruttner, and Y. Bock, "Sensitivity of GNSS to vertical land motion over Europe: Effects of geophysical loadings and common-mode errors," *J. Geodesy*, vol. 98, no. 7, 2024, Art. no. 68, doi: 10.1007/s00190-024-01856-z.

[25] J. Huang, X. He, S. Hu, and F. Ming, "Impact of offsets on GNSS time series stochastic noise properties and velocity estimation," *Adv. Space Res.*, vol. 75, no. 4, pp. 3397–3413, 2025, doi: 10.1016/j.asr.2024.12.016.

[26] K. Gobron, P. Rebischung, M. Van Camp, A. Demoulin, and O. de Viron, "Influence of aperiodic non-tidal atmospheric and oceanic loading deformations on the stochastic properties of global GNSS vertical land motion time series," *J. Geophysical Res., Solid Earth*, vol. 126, no. 9, 2021, Art. no. e2021JB022370, doi: 10.1029/2021JB022370.

[27] X. He, M. Bos, J. Montillet, and R. Fernandes, "Investigation of the noise properties at low frequencies in long GNSS time series," *J. Geodesy*, vol. 93, no. 9, pp. 1271–1282, 2019, doi: 10.1007/s00190-019-01244-y.

[28] M. R. Allen and L. A. Smith, "Monte Carlo SSA: Detecting irregular oscillations in the presence of colored noise," *J. Climate*, vol. 9, no. 12, pp. 3373–3404, 1996.

[29] M. Allen and A. Robertson, "Distinguishing modulated oscillations from coloured noise in multivariate datasets," *Climate Dyn.*, vol. 12, pp. 775–784, 1996.

[30] A. Groth and M. Ghil, "Monte Carlo singular spectrum analysis (SSA) revisited: Detecting oscillator clusters in multivariate datasets," *J. Climate*, vol. 28, no. 19, pp. 7873–7893, 2015, doi: 10.1175/JCLI-D-15-0100.1.

[31] S. Khazraei and A. Amiri-Simkooei, "On the application of Monte Carlo singular spectrum analysis to GPS position time series," *J. Geodesy*, vol. 93, no. 9, pp. 1401–1418, 2019, doi: 10.1007/s00190-019-01253-x.

[32] Y. Bian, J. Yue, V. G. Ferreira, K. Cong, and D. Cai, "Common mode component and its potential effect on GPS-inferred crustal deformations in Greenland," *Pure Appl. Geophys.*, vol. 178, no. 5, pp. 1805–1823, 2021, doi: 10.1007/s00024-021-02732-z.

[33] Y. Bian, Z. Li, Z. Huang, B. He, L. Shi, and S. Miao, "Combined GRACE and GPS to analyze the seasonal variation of surface vertical deformation in Greenland and its influence," *Remote Sens.*, vol. 15, no. 2, 2023, Art. no. 511, doi: 10.3390/rs15020511.

[34] G. Plaut and R. Vautard, "Spells of low-frequency oscillations and weather regimes in the Northern Hemisphere," *J. Atmos. Sci.*, vol. 51, no. 2, pp. 210–236, 1994.

[35] A. R. Amiri-Simkooei, "Noise in multivariate GPS position time-series," *J. Geodesy*, vol. 83, no. 2, pp. 175–187, 2009, doi: 10.1007/s00190-008-0251-8.
[36] M. Bos, R. Fernandes, S. Williams, and L. Bastos, "Fast error analysis of continuous GPS observations," *J. Geodesy*, vol. 82, no. 3, pp. 157–166, 2008, doi: 10.1007/s00190-007-0165-x.
[37] A. R. Amiri-Simkooei, "Non-negative least-squares variance component estimation with application to GPS time series," *J. Geodesy*, vol. 90, no. 5, pp. 451–466, May 2016, doi: 10.1007/s00190-016-0886-9.
[38] J. E. Gentle, *Numerical Linear Algebra for Applications in Statistics*. New York, NY, USA: Springer, 1998.
[39] A. R. Amiri-Simkooei, "Least-squares variance component estimation: Theory and GPS applications," Ph.D. thesis, Delft Univ. of Technol., Delft, The Netherlands, 2007.
[40] P. J. G. Teunissen, *Adjustment theory: An introduction*, Delft, The Netherlands: Delft Univ. of Technology, 2024.
[41] S. A. Khan, A. Aschwanden, A. A. Bjørk, J. Wahr, K. K. Kjeldsen, and K. H. Kjær, "Greenland ice sheet mass balance: A review," *Rep. Prog. Phys.*, vol. 78, no. 4, Mar. 2015, Art. no. 046801, doi: 10.1088/0034-4885/78/4/046801.
[42] G. Blewitt, W. Hammond, and C. Kreemer, "Harnessing the GPS data explosion for interdisciplinary science," *Eos*, vol. 99, no. 2, 2018, Art. no. e2020943118.
[43] K. Gobron, P. Rebischung, K. Chanard, and Z. Altamimi, "Anatomy of the spatiotemporally correlated noise in GNSS station position time series," *J. Geodesy*, vol. 98, no. 5, 2024, Art. no. 34.
[44] Z. Bao, G. Chang, L. Zhang, G. Chen, and S. Zhang, "Filling missing values of multi-station GNSS coordinate time series based on matrix completion," *Measurement*, vol. 183, 2021, Art. no. 109862, doi: 10.1016/j.measurement.2021.109862.
[45] X. Li, L. Wang, X. Qu, S. Zhang, B. Shu, and H. Xu, "A GPS multipath mitigation method in coordinate-domain considering the effects of gross errors and missing data," *Measurement*, vol. 225, 2024, Art. no. 114035, doi: 10.1016/j.measurement.2023.114035.
[46] A. Amiri-Simkooei, M. Hosseini-Asl, J. Asgari, and F. Zangeneh-Nejad, "Offset detection in GPS position time series using multivariate analysis," *GPS Solutions*, vol. 23, pp. 1–12, 2019.
[47] A. Amiri-Simkooei, "On the nature of GPS draconitic year periodic pattern in multivariate position time series," *J. Geophysical Res., Solid Earth*, vol. 118, no. 5, pp. 2500–2511, 2013.
[48] J. Ray, Z. Altamimi, X. Collilieux, and T. van Dam, "Anomalous harmonics in the spectra of GPS position estimates," *GPS Solutions*, vol. 12, pp. 55–64, 2008.

Fatemeh Esmaeili received the M.Sc. degree in geodesy from the University of Isfahan, Isfahan, Iran, in 2019, where she is currently working toward the Ph.D. degree in geodesy with the Department of Geomatics Engineering, Faculty of Civil Engineering and Transportation.

Her research area focused on data analysis methods and techniques with an emphasis on applications to geodetic data.

Hamid Mehrabi received the Ph.D. degree in geodesy from the K.N Toosi University of Technology, Iran, in 2017.

He currently serves as an Assistant Professor with the Department of Geomatics Engineering, University of Isfahan, Isfahan, Iran. His research focuses on areas, such as InSAR and GNSS position time-series analysis, deformation analysis of the crust, and estimation theory.

Seyed Mohsen Khazraei received the Ph.D. degree in geodesy from the University of Isfahan, Iran, in 2021.

He currently serves as an Assistant Professor with the Department of Surveying Engineering, Jundi-Shapur University of Technology, Dezful, Iran. His research focused on GNSS position time-series analysis. He worked on developing techniques encompassing both data-adaptive methods, such as SSA, and LS-based approaches.

Alireza Amiri-Simkooei received the graduated degree in geodesy from the Mathematical Geodesy and Positioning Group at Delft University of Technology, The Netherlands, in 2007.

His doctoral research focused on least-squares variance component estimation with applications to GPS data. He is an Associate Professor with the Department of Control and Operations, Delft University of Technology, Delft, The Netherlands. His research interests include GNSS position time-series analysis, optimization and estimation theory, and stochastic modeling and processes.